On the Performance of Highly Aggressive Inter Compressor Ducts

Stefan Fritz and Dr.-Ing. Alexander Hergt
Stefan.fritz@dlr.de
German Aerospace Center
Institute of Propulsion Technologies | Department of Fan and Compressors
Cologne
Germany

David Bresemann, Dr.-Ing. Mario Eck, Prof. Dieter Peitsch
TU Berlin
Institute of Aeronautics and Astronautics | Chair of Aero Engines
Berlin
Germany

ABSTRACT

The improvement of jet engine components can lead to an escape of the understood design space. In particular, the trend towards short and therefore highly aggressive inter compressor ducts (ICD) extends the traditional design space. Potential benefits in terms of fuel savings due to a reduction in engine weight are in contrast to a more complex flow field. Many studies consider the secondary flow system of highly aggressive ICDs at the design point but there is a lack of off-design considerations. To fill this gap, the present study investigates in detail the off-design performance of the new German Aerospace Center (DLR) test case. Firstly, CFD simulations of different typical operating points allow detailed considerations of the flow field under off-design conditions. Secondly, a variation of the inlet conditions describes the sensitivity of highly aggressive ICDs to different low-pressure compressor operating points. Finally, the comparison of the CFD stagnation pressure loss with the loss predicted by a preliminary off-design method validates the use of traditional off-design prediction during the preliminary design of highly aggressive ICDs.

Keywords: Inter Compressor Duct; Flow Separation; Compressor Aerodynamics

NOMENCLATURE

ADP	aerodynamic design point
HPC	high-pressure compressor
ICD	inter compressor duct
LE	leading edge
LPC	low-pressure compressor
ma	mass-averaged
MTO	maximum take-off
OGV	outlet guide vane
OP	operating point
sep	separated
ssw	wall shear stress
TE	trailing edge

Symbols

A	area
$\dot{m}$	mass flow rate
p	pressure
T	Temperature
t	stagnation state
ω	pressure loss coefficient

1. INTRODUCTION

The compressor of modern civil jet engines can be divided into the three distinct components the fan, the intermediate-/low-pressure compressor (LPC) and the high-pressure compressor (HPC). The LPC and HPC operate on different radii to enable them to operate at optimum rotational speeds while remaining within mechanical limits. Both components are connected by the inter compressor duct (ICD). The main aerodynamic task of an ICD is to guide the core mass flow to lower high-pressure spool radii. Most ICDs include struts providing structural integrity and the ability to route pipes for secondary systems like the oil system and the secondary air system.
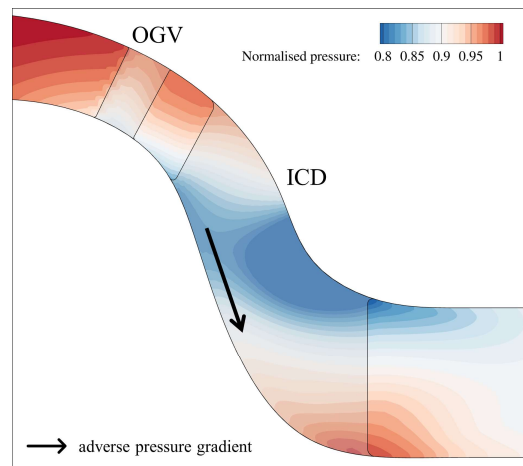

Figure 1: Pressure field in an aggressive ICD.

The flow field of an ICD is mainly influenced by the curvature of the duct. Flow is accelerated and decelerated on convex and concave end walls, respectively. Axial and radial pressure gradients develop due to the S-shaped nature of the ICD, as shown in Figure 1. This results in a very complex flow field where the hub boundary layer experiences an adverse pressure gradient causing separation on the side walls and the strut surfaces as described by Fritz [1].

Shortening ICDs would be beneficial for future aircraft engines as the climate impact can be reduced by decreasing the engine weight. Reducing the length of an ICD leads to an increased turning of the flow, which in turn increases the risk of separation on the ICD hub wall. Based on oil flow visualizations, Naylor [2] and Karakasis [3] showed that the flow no longer follows the duct contour in the rear part of the ICD. In order to expand the design space towards shorter and more aggressive ICDs, methods must be developed to influence the flow, especially in the critical hub area.

One solution to reduce the risk of flow separation is to apply means of passive flow control like the non-axisymmetric end wall contouring, investigated for example by Stürzebecher [4]. These methods have the disadvantage that they cannot be modified during operation. However, during flight operation, jet engines experience different operating conditions. Active flow control (AFC), on the other hand, has the advantage of being adjustable within the operating range to the cost of a rise in system complexity as well as the additional weight of the actuator and the supply system.

Much effort has been spent by e.g. Fritz [1], Karakasis [3] or Kasper [5] to describe the secondary flow within aggressive ICDs at design flow conditions. A first attempt to include the performance at different operating points while optimizing the ICD geometry was conducted by Dygutsch [6]. Dygutsch showed, that the losses at different operating points depend to different degrees on the shortening of the ICD. A more detailed evaluation of the differences in the flow field at different operating points cannot be found in literature.

In order to develop efficient operating strategies for active flow control methods, it is necessary to enhance the understanding of the off-design performance of highly aggressive ICDs. To fill this gap, the aerodynamic performance of ICDs at different operating points (ADP, MTO and idle) is investigated in detail on a new highly aggressive ICD design. This test case is specifically designed to be separated at the hub in the second bend, providing the possibility to demonstrate the ability of flow control methods to suppress this separation. A sensitivity study is also carried out to determine the response of a highly aggressive ICD to varying inlet conditions. Finally, a preliminary design method by Walsh and Fletcher [7] for the off-design performance prediction of ICDs is applied to validate its application for highly aggressive ICDs. In summary, this paper answers the question of how the flow structure of a highly aggressive ICD changes at different operating points.

2. TEST CASE DESIGN

Research over the past decades has led to many different ICD designs. However, they all have several characteristics in common. The flow field of ICDs is strongly influenced by the S-shaped nature of the flow path. The curvature causes a strong adverse pressure gradient at the ICD hub, which can cause separations. Because of this large pressure gradient, the flow is no longer able to follow the hub contour anymore. The result is a strong cross-flow in the rear part of the ICD. Consequently, the hub boundary layer shifts on the strut and is transported to a higher radius. According to studies of ICDs operating under engine-like flow conditions, e.g. by Stürzebecher [4], Kasper [8], Dygutsch [6], Jonsson [9] or Fritz [1], the flow field downstream of the ICD is asymmetric. The design of the new test case was mainly driven by the need to reproduce these characteristics.

The Institute of Propulsion Technologies of the German Aerospace Center (DLR) developed this new highly aggressive strutted ICD test case. In order to demonstrate the ability of flow control methods to eliminate separations, this test case was specifically designed to have severe separations in the rear part of the ICD passage. These separations were mainly caused by a large deceleration due to an area expansion in the second bend. A row of LPC-OGVs was also designed upstream of the ICD. The profiles used for the OGV are symmetric NACA0012 profiles. This row shall address the reenergizing effect of the hub boundary layer by the OGV secondary flow system as described by Karakasis [3]. The asymmetry of the ICD inlet flow field was achieved by introducing a slight swirl to the flow (clock-wise in flow direction) close to the hub by staggering the lower part of the OGVs. This measure guarantees the typical asymmetric ICD outlet flow field.
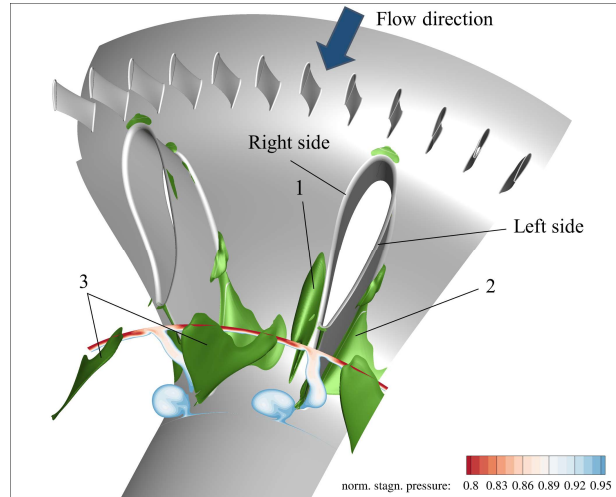
Figure 2: Flow field of the new ICD test case.

Two passages of the ICD test case are shown in Figure 2. The green area represents the boundary surface enclosing the area affected by negative axial velocity and therefore, indicating flow separation. The separations can be divided into three different types. The axial pressure gradient at the hub causes a separation in the middle of the passage (1). A hub-corner separation (2) appears on the left side of the strut (defined according Figure 2 in flow direction), which is typical for aggressive ICDs. The separation occurs on this side of the strut because this side is flowed against by the slight inlet swirl. The horse shoe vortices of the strut cause further separations at the shroud (3) downstream of the ICD. In summary, this new test case is highly separated in the rear part and, thus a valid case to demonstrate the capability of future flow control methods to suppress separations.

The slice downstream of the ICD displays the normalized stagnation pressure distribution. Regions colored red had experienced high losses during passage through the test section, while regions with lower losses are transparent to provide a better view on the separations. The outlet flow field of the ICD displays an asymmetrical character as shown by the stagnation pressure distribution. Finally, the test case fulfills all design objectives and can replicate engine-like flow conditions.

3. NUMERICAL SETUP

The numerical domain represents one ICD passage with the corresponding 6 LPC-OGVs. NUMECA AutoGrid was used to generate structured multiblock meshes for the present study. All meshes are designed as low-Reynolds meshes with $y^+ \approx 1$. Figure 3 shows the scope of the numerical setup. The outlet is placed at a sufficient distance from the ICD to allow the mixing out of the shroud separation. In this way, numerical instabilities can be avoided. The numerical simulation is evaluated in three different planes. The inlet plane is also the evaluation plane P1. The plane P2 is located between the OGV and the ICD and is later used to determine the loss coefficient of the ICD. Behind the ICD, there is another plane P3. This plane allows an evaluation of the ICD outflow by a planar distribution of the flow properties. The study by Fritz [1] showed that this plane is a powerful tool to evaluate the flow structures inside an ICD.
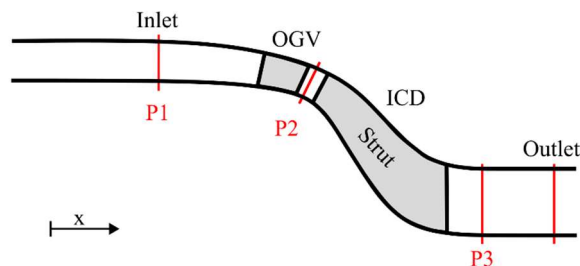

Figure 3: Evaluations planes in the numerical setup.

The mesh independency is evaluated with the mass-averaged pressure loss coefficient ω_{ICD} (Eq. 1) and the separated end wall area A_{sep}. The separated end wall area A_{sep} is the sum of all wall cells in the ICD with a representative wall shear stress ssw below 0. The representative wall shear stress ssw (Eq. 3) is the magnitude of the wall shear stress vector $\overrightarrow{ssw}$. The sign of the representative wall shear stress is determined by the sign of the axial component of the tangential velocity vector $v_{\parallel,x}$. This method also identifies the strut leading and trailing edge as separated. The area of negative wall shear stresses at the LE and TE are deducted from the sum to only balance the separations caused by the pressure gradient in the duct.

$$\omega_{ICD} = \frac{p_{t,P2,ma} - p_{t,P3,ma}}{p_{t,P2,ma} - p_{P2,ma}} \qquad (\quad 1\quad)$$

$$A_{sep} = \sum_{ICD} A_i(ssw < 0) \qquad (\quad 2\quad)$$

$$ssw = sign(v_{\parallel,x}) \cdot |\overrightarrow{ssw}| \qquad (\quad 3\quad)$$

Six different meshes were considered to proof the mesh independency. The number of cells varies from 1.5 million to 14 million cells. Figure 4 shows the results of the mesh convergence study for the pressure loss coefficient ω_{ICD} and the separated end wall area A_{sep} without strut LE and TE regions. The size of the separations is highly dependent on the number of cells. Therefore, the mesh with around 9 million cells was chosen for further studies as it provided a good compromise between numerical accuracy (about 2 % deviation in the pressure loss coefficient ω_{ICD} to the finest mesh) and simulation time. In addition, the mass flow controller used tends to oscillate as the number of cells increases cell number which causes convergence problems.
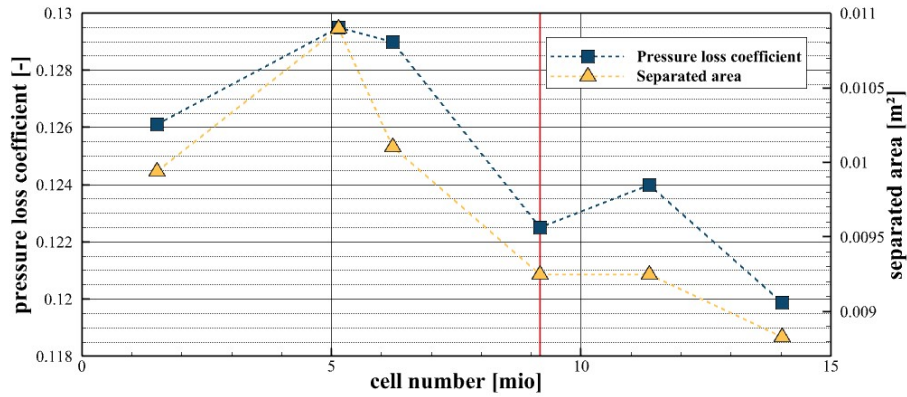

Figure 4: Results of the mesh convergence study.

The flow solver for the numerical simulation is TRACE [10], which was developed by the DLR's Institute of Propulsion Technologies. TRACE solves the compressible RANS equations with the finite-volume method. In a previous study on a similar configuration, Fritz [1] showed that the Menter SST turbulence model [11] predicts the size of separations in the ICD in a very good agreement with experimental results. Therefore, this turbulence model is used for the numerical simulations. Fritz [1] also showed, that the application of a transition model has an effect on the flow field inside the ICD. However, the differences between the applied transition models available in TRACE (the three transition models proposed by Langtry and Menter [12]) are negligibly small. For the current study the Menter 2004-1 transition model is selected. The CFL number is 50 for every simulation. The inlet boundary conditions are adapted from the measurements of Kasper [8], where a detailed measurement campaign was conducted on a similar setup. The radial stagnation pressure profile (Fig. 9 in Kasper [8]) includes a boundary layer on both end walls. A purely axial inflow is prescribed and the turbulence intensity is set to a radially constant value of 1.5 %. The stagnation temperature corresponds to the measured value of around 300 K. A prescribed mass flow rate in combination with a mass flow controller is used as outlet boundary condition.

4. PERFORMANCE ON DIFFERENT OPERATING POINTS

The investigation of the performance of the present highly aggressive ICD starts with the consideration of the ADP as benchmark for further studies. Then, the extreme cases of the engine performance in terms of thrust are investigated. The operating point delivering the maximum thrust is Maximum Take-Off (MTO) whereas the minimum thrust point is idle. **Table 1** characterizes the Mach and Reynolds number levels of the three investigated operating points. The definition of the operating points is based on the studies of Kasper [8] and Wallin [13].

Table 1
Characterization of the inlet conditions of the different operating points

Case	Mach number	Reynolds number
ADP	Medium	Medium
MTO	Medium	High
Idle	Low	Low

4.1 Aerodynamic Design Point (ADP)

Figure 5 shows the flow field of the ICD at ADP conditions. The left side visualizes the nature of the flow separations. The green line (SL1) marks the onset of the hub corner separation on the left side of the strut whereas the blue line (SL2) marks the onset of the passage separations. These separation lines are introduced to compare the onset of the separations for the different operating points.

Three distinct separations can be observed. The complete rear part of the hub is almost separated in the left part of the passage (in streamwise direction), which starts with a corner separation. In the other part of the passage, a well defined circular separation occurs a bit away from the hub-strut corner. There is also a large separation at the shroud.

The right side shows the planar distribution of the pressure loss coefficient ω_{ICD} (Eq. 1) after the ICD (P3 in Figure 3). The whole tip region experiences high losses, while a well defined circular loss region (A) occurs at the hub. In the middle of the passage, the wake of the strut (B) is clearly recognized. The flow field is also influenced by the OGV wakes, for example at C.
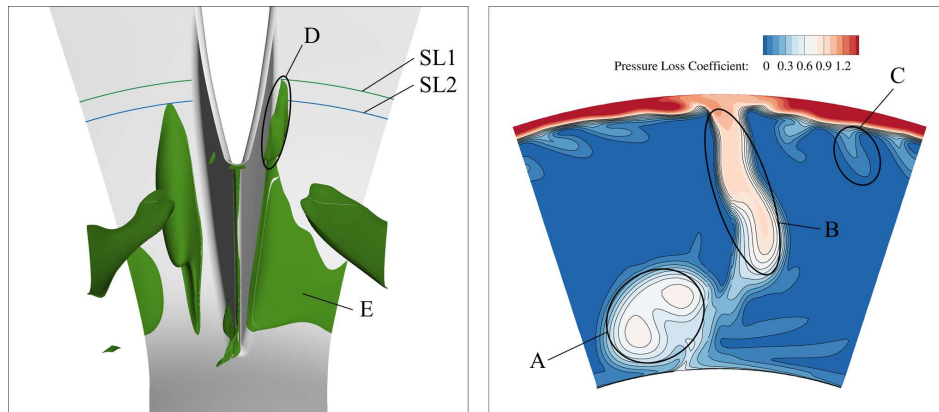

Figure 5: Flow field and ICD outlet loss distribution (in P3) for ADP.

The origin of the main three loss regions is further investigated in Figure 6. Figure a) shows the flow field on the right side of the strut (in streamwise direction) and figure b) the flow field on the other side. The origin of the loss regions of the planar distribution in Figure 5 is visualized by differently colored streamlines. The loss regions are marked by black iso-lines behind the strut trailing edge.

The different streamlines underline that the flow field of the ICD is very asymmetric. The flow field of the right part of the ICD passage (Figure 6 a)) is determined by two counter rotating vortices (yellow (1) and orange (2)). The hub boundary layer cannot withstand the huge adverse pressure gradient and consequently separates. This passage separation causes both vortices. The loss region (A) at the hub is related to these vortices.
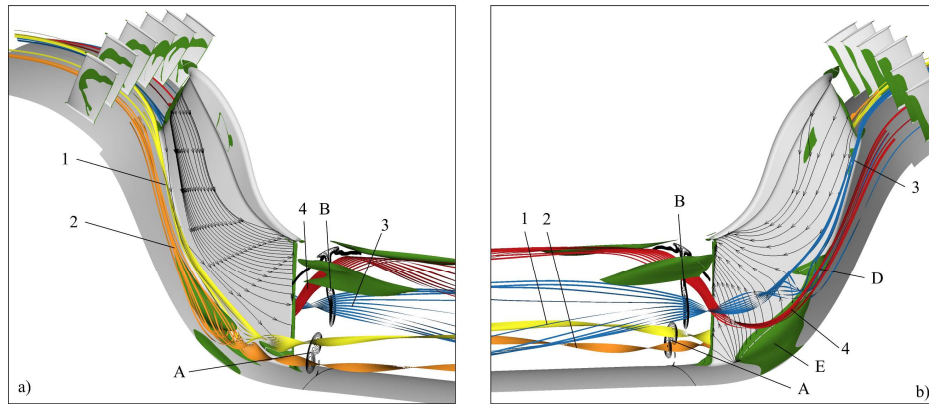

Figure 6: Detailed view on the ICD flow field and vortex system.

On the other side, the horse shoe vortex (blue (3)) detaches from the hub corner and causes a hub corner separation (D). The losses near the strut wake (B) are related to this vortex. The red streamlines (4) characterize the behavior of fluid which exhibits the strong separation at the hub (E). The hub boundary layer cannot withstand the strong pressure gradient at the hub and escapes to the left side of the strut. A strong cross-flow occurs in combination with a separation. Once arrived at the strut, the low momentum fluid is concentrated on the surface. Furthermore, the fluid shifts to the shroud because of the strong radial pressure gradient in the second bend. This shift of hub boundary layer to the shroud is a very typical phenomenon of highly aggressive ICDs as already discovered by Fritz [1].

The black streaklines on the strut's surface underline the previous findings. The flow on the right side of the strut can still follow the contour, whereas the flow of the opposite side experiences a strong cross flow. Also, the shift of low momentum fluid from the hub over the left strut side to the shroud is clearly visible.

4.2 Maximum Take-Off (MTO)

The Reynold number for MTO is 50 % higher than for ADP. The Mach number remains the same. Figure 7 shows again the size of separations (left) and the loss distribution (right). At first glance, both plots are very similar to the ADP. Only slight differences can be observed. Firstly, the onset of separation for both the passage and the hub corner separation is slightly delayed (in comparison to SL1 and SL2 of the ADP). Also, the separated volume is slightly smaller. Secondly, the losses, especially in the vortex cores (A) are lower. As shown in Figure 11, the pressure loss coefficient for MTO is about 0.1 percentage points (Δ%) lower. Therefore, the influence of Reynolds number on the separations is negligible, especially in comparison to the Mach number influence, investigated in chapter 5. This means that the inertial forces are already superior to the viscous forces at ADP.
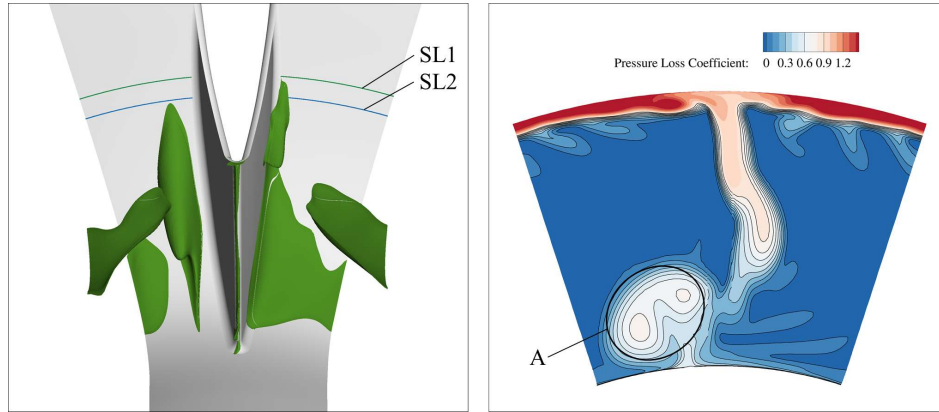
Figure 7: Flow field and ICD outlet loss distribution (in P3) for MTO.

4.3 Idle

The idle operating point is characterized by a very low inlet Mach number, mass flow rate and pressure level. Figure 8 shows the separations and the loss distribution at idle. Obviously, the flow field is more asymmetric than for the other operating points. The strong cross flow is also more pronounced as can be seen from the shape of the large hub separation (A). Furthermore, the shroud separation (B) is only on one side of the passage. The loss regions around the wake (C and D) are larger whereas the losses in the hub region (E) are much smaller and closer to the hub. The onset of the hub-corner separation, caused by the hub horse shoe vortex is located further upstream than for the other operating points (SL1) and also has more volume.
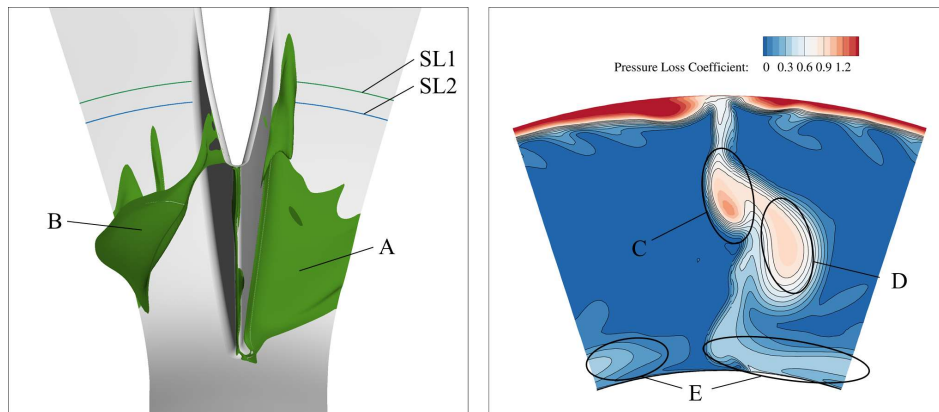

Figure 8: Flow field and ICD outlet loss distribution (in P3) for idle

Figure 9 shows the complex vortex system of the ICD at idle. Three distinct vortices can be observed. The yellow streamlines (1) represent fluid that is part of the hub separation and the strong cross flow. This fluid flows over the rear part of the strut surface. Behind the trailing edge, the hub separation losses are well defined as a circular high loss region (C). In contrast to the ADP, the low momentum fluid from the former hub boundary layer is not pushed towards the shroud. The hub corner separation induces a vortex, which is highlighted by the green streamlines (2). This vortex is responsible for the large loss region in the center of the duct (D). The blue streamlines (3) form the edge of the hub separation. This fluid does not experience separation but a strong cross flow. After flowing over the strut fillet, this fluid forms another vortex. In contrast to the other vortices, this one causes only slight losses.
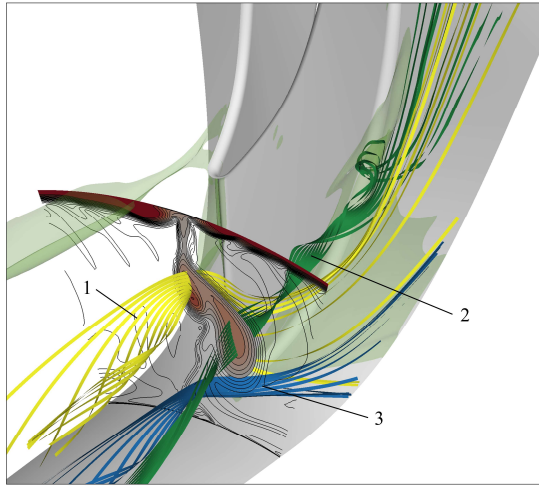
Figure 9: Idle vortex system.

4.4 Summary

Finally, Figure 10 and Figure 11 summarize the findings of the off-design considerations. Figure 10 compares the size of the separations in terms of relative difference to the ADP (Eq. 4).

$$\Delta A_{\mathrm{OP}} = \frac{A_{\mathrm{OP}} - A_{\mathrm{ADP}}}{A_{\mathrm{ADP}}} \qquad\qquad (\quad 4 \quad)$$

Overall, the size of the separation at idle condition is with almost 8 % significantly smaller. But the size of the hub separation is larger. At MTO, all separations are a bit smaller, as already seen in the 3D visualization (Figure 7).
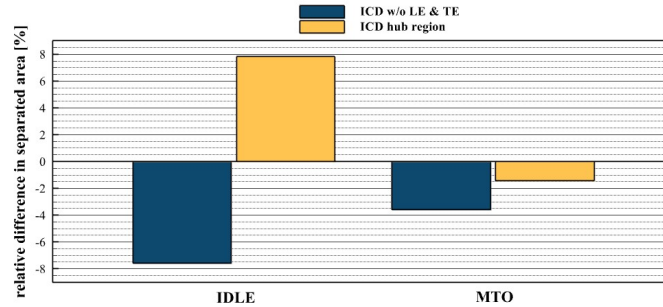

Figure 10: Difference in separated surface area in relation to ADP.

Figure 11 shows the differences in the pressure loss coefficient of MTO and idle in relation to the ADP in terms of percentage points. The idle losses are about 1.5 Δ % lower although the hub separations are almost 8 % larger. The cause of the lower losses is mainly the significant lower inlet Mach number. The MTO losses are almost identical to the ADP losses as the inlet Mach number is the same for both cases. The influence of the larger Reynolds number is negligible at less than 0.1 Δ%.
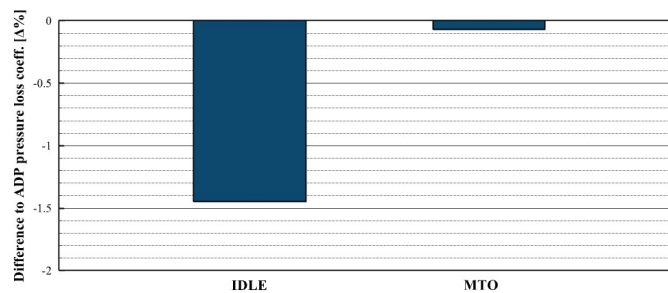
Figure 11: Difference in pressure loss coefficient ω_{ICD} in relation to ADP.

5. SENSITIVITY STUDY

The operating point of an LPC often changes during operation. As the inlet pressure and the mass flow rate vary, these changes have a direct effect on the downstream ICD. To investigate the sensitivity of the ICD flow fields to changes in the LPC operating point, four different cases (listed in **Table 2**) are set up by varying either the inlet stagnation pressure or the mass flow rate by ±5 % up to the ADP condition. The cases are chosen in such a way that they simulate the extreme cases of an operating point change of an LPC on a speed line. For a subsonic compressor, the speed lines in a compressor map close to the surge line are almost horizontal. In this case, the inlet pressure of an ICD would be constant. Only the mass flow rate would vary. Next generation LPCs where the rotational speed of the LPC is decoupled from the fan, will be designed with a transonic first stage. Transonic speed lines are nearly vertical because a change in backpressure only affects the position and strength of the shock, not the mass flow rate. Speed lines are also vertical when the LPC is choked. A graphical interpretation of the different cases is shown in Figure 15.

Table 2
Inlet condition of the different cases investigated in the sensitivity study

Case	Stagnation pressure	Mass flow rate	Mach number	Reynolds number
1	− 5 %	ADP	+ 6.7 %	+0.3 %
2	+ 5 %	ADP	− 6.1 %	− 0.3 %
3	ADP	− 5 %	− 6.1 %	− 5.0 %
4	ADP	+ 5 %	+6.7 %	+5.3 %

The duct flow capacity $\dot{m}_{red}$ (Eq. 5) depends on the mass flow rate $\dot{m}$, the stagnation temperature T_t and the stagnation pressure p_t. Reducing the stagnation pressure or increasing the mass flow rate will result in an increase in the duct flow capacity. Thus, the duct flow capacity and the inlet Mach number are the same for cases 1 and 4 as well as for cases 2 and 3.

$$\dot{m}_{red} = \dot{m}\ \frac{\sqrt{T_t}}{p_t} \qquad\qquad (\quad 5 \quad)$$

The mass flow rate has a direct effect on the Reynolds number. The Reynolds number changes in the same order as the mass flow rate. In contrast, the difference in Reynolds number for cases 1 and 2 where the inlet stagnation pressure is changed, is only Δ0.6 %. The influence of compressibility effects on the Reynolds number is therefore very small.
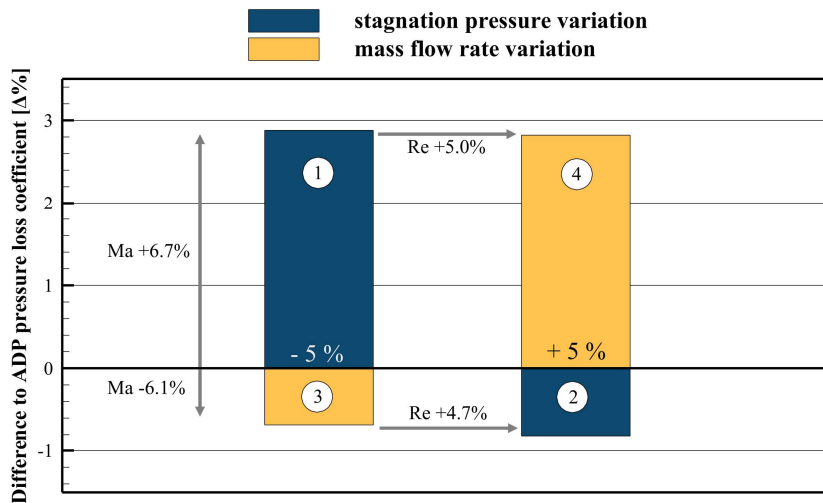

Figure 12: Differences of the pressure loss coefficient in relation to the ADP in percent points.

Figure 12 shows the difference between the pressure loss coefficient (Eq. 1) of the specific case and that of the ADP in percentage points (Δ%). Increasing the Reynolds number by 5 % reduces the losses only slightly (around 0.1 Δ%). Thus, the Reynolds number has a negligible effect on the pressure loss coefficient. This finding confirms the results of section 4.4 where no influence of the Reynolds number was also found. The main influence on the losses of the ICD is the inlet Mach number. In addition, an increase in Mach number causes a significantly greater increase in losses than a reduction in Mach number would reduce losses. Further investigations are only considering a Mach number variation by changing the stagnation pressure (case 1 and 2) at almost constant Reynolds number.

Figure 13 shows an azimuthal averaging of the meridional Mach number on the meridional plane (S2 plane). For the lower Mach number, the flow near the hub in the second bend is very slow. In case 4, the flow near the hub is faster, but there is a supersonic region (marked by the black line) on the casing. The ICD operates close to choking conditions. A further increase of the inlet Mach number would lead to ICD choking. Hence, when designing an ICD, it is very important to select the smallest area that is large enough to prevent the ICD from choking before the LPC. The ICD should not be the limiting factor for off-design operations. The smallest area depends not only on the flow path, but also on the thickness distribution of the strut. This finding also highlights the importance of the cross-module design introduced by Dygutsch [6].
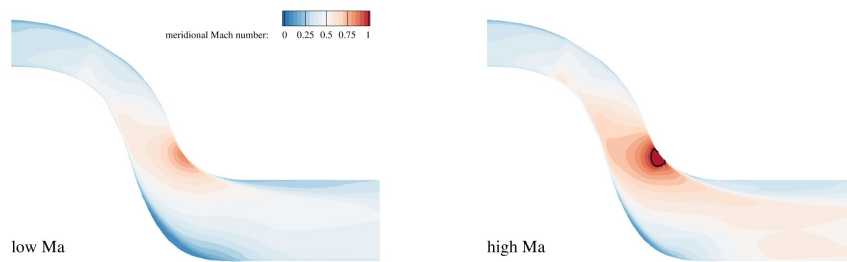

Figure 13: Contour plot of the meridional Mach number for the low and high Mach number case.

Figure 14 provides a detailed view on the ICD flow field for case 2 (lower Mach number) and case 1 (higher Mach number). The green areas are iso-surfaces of negative axial velocity and therefore a measure of flow separations. The nature of the separation is different for the two cases. The hub separation is larger for case 2 while the shroud separation is significantly smaller compared to case 1. In case 1, the shroud separation is caused by the fluid being too fast to follow the end wall curvature. In summary, the separation shifts from hub to shroud as the inlet Mach number increases.

To relate the planar distribution of the pressure coefficient of plane P3 (plots e) and f)) to the 3D plot (plots a), b), c) and d)), the plane P3 is also shown but with a slight modification. Regions with low pressure loss coefficients close to 0 are transparent to give a better view on the separations. The onset of separation occurs in an OGV wake in case 2, as indicated by the red (1) and blue (2) streamlines in plot a). The right side leg of the horse shoe vortex (green (3)) does not affect the onset of separation. In contrast to case 1, the losses have a larger circumferential extension (A in plot e) compared with C in plot f)). In plot b), the separation is caused by a combination of the OGV wake (blue (4)) and the right side leg of the strut horse shoe vortex (red (5)). The cores of these vortices are clearly visible as well defined loss regions in plot f) (4 and 5). In summary, the separation mechanism changes at different Mach numbers.

The plot c) and d) of Figure 14 also shows strut surface streaklines. The flow field in both cases is very similar as the strut surface exhibits a strong cross-flow (visualized by the streaklines). The yellow streamlines (6 and 8) underline this cross-flow. The low momentum fluid of the hub boundary layer cannot withstand the strong pressure gradient in the rear part, and escapes to the left side of the strut. The low momentum fluid flows over the strut surface and accumulates at the shroud. This shift of boundary layer fluid from hub to shroud is very typical for highly aggressive ICDs as already shown in Fritz

[1]. The blue streamlines (7 and 9) represent the left leg of the strut horse shoe vortex. This vortex is also pushed upwards by the radial pressure gradient in the second bend and is responsible for the high loss regions in the center of the duct (B and D).
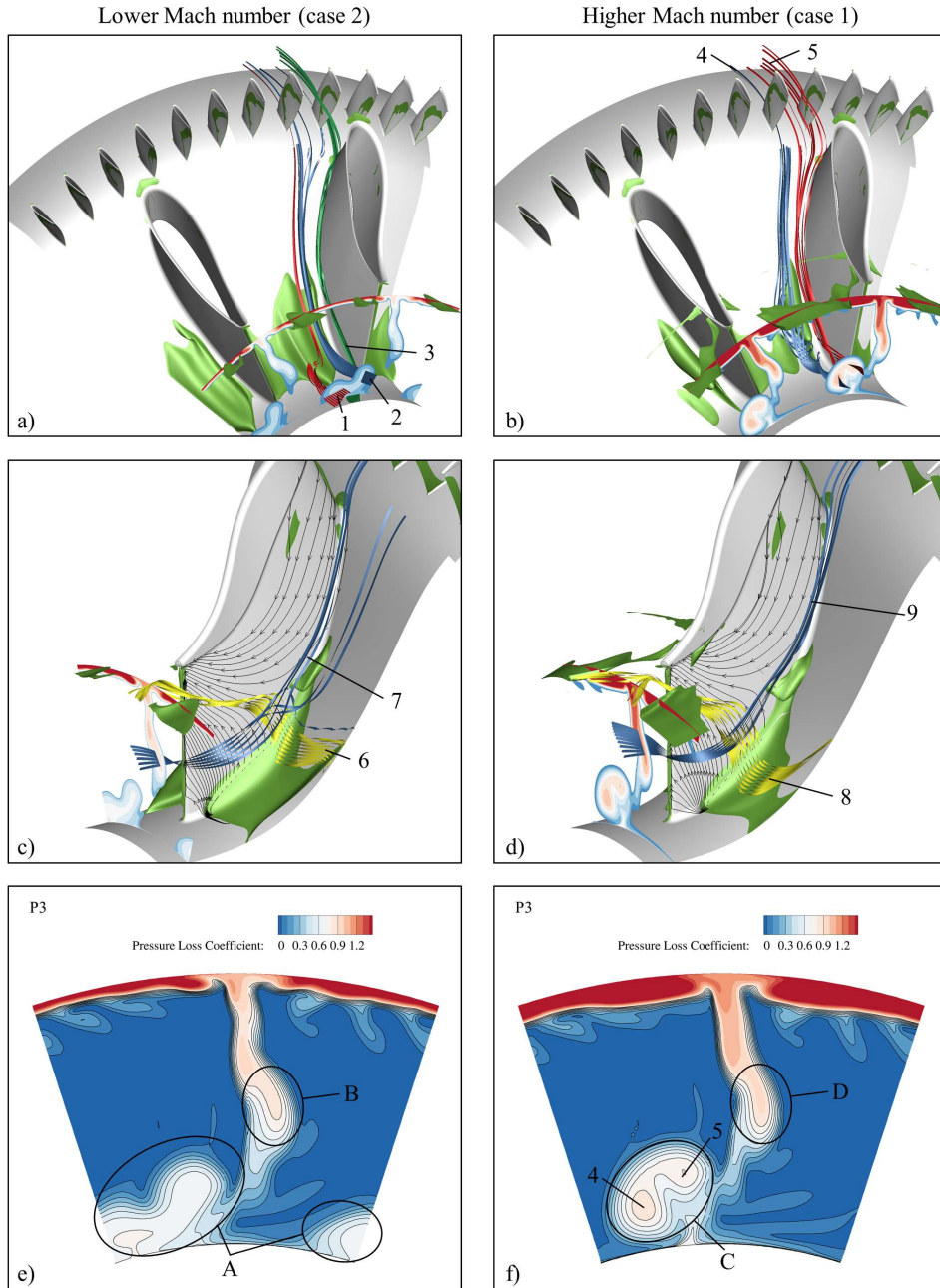

Figure 14: Comparison of the flow field of different Mach numbers.

The results of the sensitivity study are summarized in a kind of compressor map in Figure 15. The grey areas define possible operating regions of realistic speed lines. Summarizing, as the operating point moves towards the choke line (larger Mach numbers), the losses increase and a counter rotating vortex pair emerges. Also, supersonic regions are possible. In the other direction, as the Mach number decreases, the losses also decrease but there are large separations at the hub.
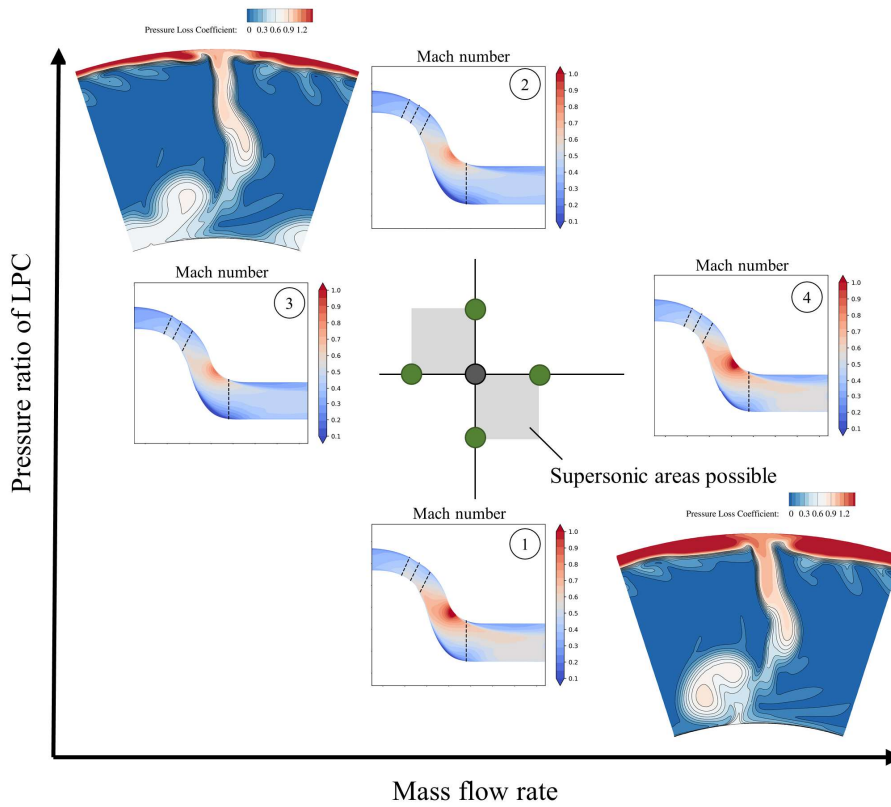
Figure 15: Results of the sensitivity study.

6. COMPARISON TO A PRELIMINARY DESIGN CORRELATION

The first step in the development of a new jet engine is the preliminary design. Preliminary design uses simple methods to find the optimum engine design. This design stage is based on empirical values of the traditional design space. These engines have very conservative ICD designs in terms of slope as shown for example by Kasper [7]. However, since the design space is extended by highly aggressive ICDS, the flow field of these ICD differs significantly from traditional designs. Friction losses should be lower due to the smaller wetted surface. On the other hand, secondary losses should be higher due to the complex vortex system and flow separations as already considered in the previous chapters. This chapter examines whether the off-design performance of a highly aggressive ICD can be predicted using preliminary design methods.

At first, a design point calculation has to be conducted to fix the geometry of the new engine. Herein, the stagnation pressure loss $\Delta p_t / p_{t,in}$ (Eq. 6) is the major parameter as it defines how the stagnation pressure changes between LPC and HPC. This pressure loss only depends on the geometry, the inlet Mach number and the inlet swirl angle [7].

$$\frac{\Delta p_t}{p_{t,in}} = \frac{p_{t,P2} - p_{t,P3}}{p_{t,P2}} \qquad\qquad (\quad 6 \quad)$$

Without having detailed information about the ICD geometry, typical values for the pressure loss in the ICD can be prescribed. Walsh and Fletcher [7] suggest that a typical stagnation pressure loss for an ICDs at its ADP is 1-2 %. As shown in Figure 16 the CFD stagnation pressure loss of the ADP is almost in the middle of the proposed range. Therefore, the suggested range can also be used as a first guess in preliminary design consideration for a highly aggressive ICD.
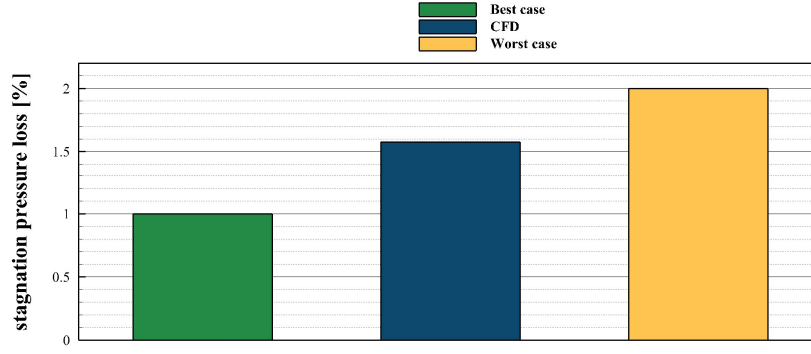
Figure 16: Typical ICD losses by Walsh and Fletcher [7] in comparison to the ADP loss of the DLR-ICD.

After fixing the ADP, off-design considerations can be conducted. Walsh and Fletcher [7] suggest a method to predict the stagnation pressure loss for different off-design operating points which is described in the following. Assuming that inlet swirl is not desired at the ICD inlet, the loss depends only on the geometry. For off-design calculation where the geometry is fixed, the stagnation pressure loss is only a function of the inlet Mach number, which also has been shown in chapter 5. Assuming now, that the squared duct flow capacity is proportional to the dynamic pressure (Eq. 7), the pressure loss coefficient of the ADP $\omega_{ICD,ADP}$ can be extrapolated to any off-design point. Therefore, the pseudo loss coefficient α is calculated using Eq. 8 to avoid interpolation. Finally, the stagnation pressure loss of an off-design point can be calculated with the known ICD inlet conditions using Eq. 9.

$$(\dot{m}_{in}\sqrt{T_{t,in}}\,/p_{t,in})^2 \propto (p_{t,in} - p_{in})/p_{t,in} \tag{7}$$

$$\alpha = \frac{\omega_{ICD,ADP} \cdot \left(1 - \dfrac{p_{in}}{p_{t,in}}\right) * 100}{(\dot{m}_{in}\sqrt{T_{t,in}}\,/p_{t,in})^2} \tag{8}$$

$$\frac{\Delta p_t}{p_{t,in}}\,[\%] = \alpha \cdot (\dot{m}_{in}\sqrt{T_{t,in}}\,/p_{t,in})^2_{Off-Design} \tag{9}$$

Figure 17 compares the predicted stagnation pressure losses (yellow bars) to the losses of the CFD simulation (blue bars). The predicted losses are in very good agreement to the CFD losses. The predicted losses are slighltly higher. Therfore, using this off-design correlation is a prediction on the conservative side. In summary, the method (Eq. 8 and 9) suggested by Walsh and Fletcher [7] is also able to predict the off-design performance of an aggressive ICD while preliminary design.
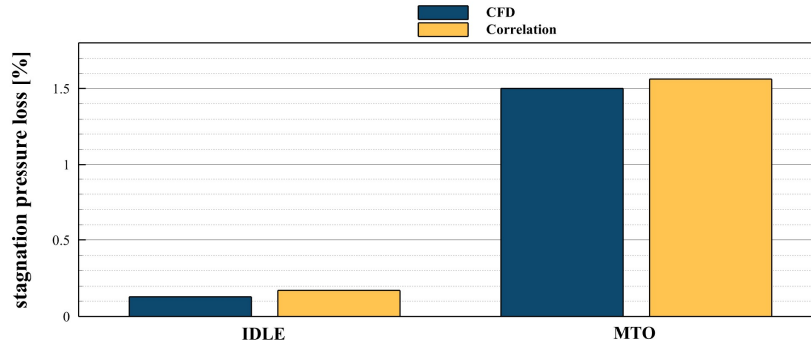

Figure 17: Comparison of the predicted and the calculated stagnation pressure loss.

7. CONCLUSIONS

A detailed study has been conducted to evaluate different aspects of the off-design performance of highly aggressive ICDs. Firstly, the new highly aggressive DLR-ICD has been introduced. The flow field on three different operating points has been analyzed in detail. Furthermore, the sensitivity of operating point changes of the upstream LPC on a speed line has been investigated. Finally, a correlation to predict the off-design performance has been applied to validate its suitability for highly aggressive ICDs. The key findings of the present study are:

1. As shown in the sensitivity study, the flow field and the pressure loss of an aggressive ICD depends only on the inlet Mach number. The influence of the Reynolds number is negligible small.
2. Furthermore, as the inlet Mach number slightly increases, the ICD is prone to choke. Therefore, the smallest area of a next generation ICD has to be chosen in a way that the ICD is not choking in off-design.
3. The off-design performance correlation from Walsh and Fletcher [7] provides very accurate results for different operating points.
4. Large separations at the hub occur for every considered operating point because of the adverse pressure gradient. At idle, almost the complete hub surface is separated. By lowering the Mach number, the hub separation becomes more severe. Thus, further studies should focus on stabilizing the hub boundary layer with flow control methods for every operating point.

Furthermore, experimental investigations for validation of the numerical analyzes are planned to take place at the Chair of Aero Engines at the Technische Universität Berlin. The test rig in Figure 18 represents a downscaled model of the before mentioned ICD. The measurement planes in the experimental setup reflect the positions of the evaluation planes of the numerical setup. The test rig is specifically designed to incorporate fifteen circumferential measurement positions for static pressure at the inlet and the outlet plane. Additionally, wake flow measurements with a miniature five-hole probe upstream and downstream of the ICD domain will be conducted.
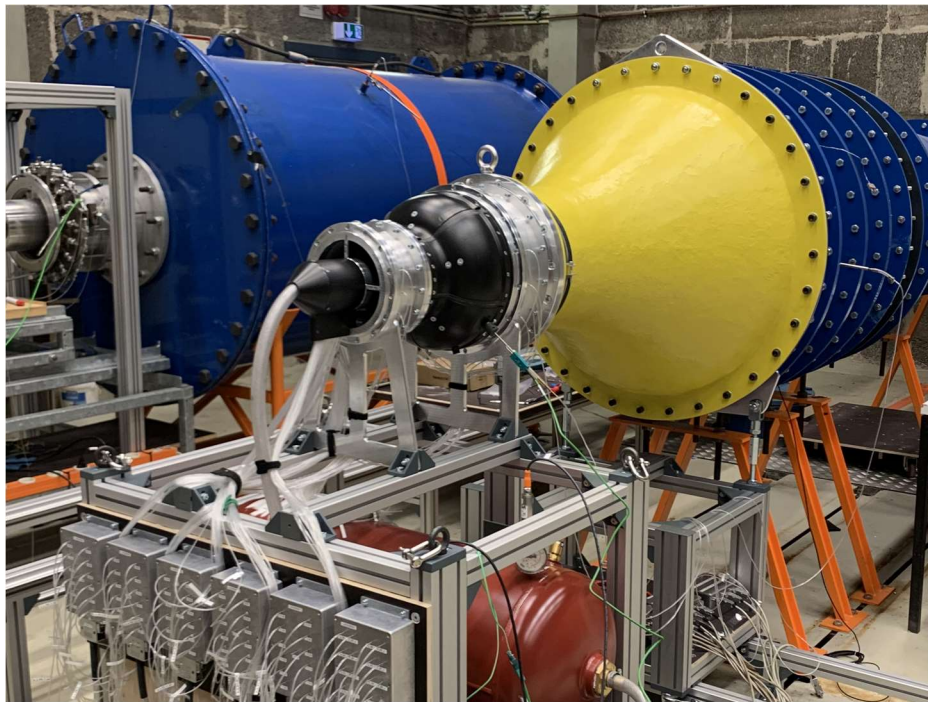

Figure 18: ICD test rig at the Chair of Aero Engines at the TU Berlin.

ACKNOWLEDGMENTS

REFERENCES

[1]   Fritz, S., Dygutsch, T., Kasper, A., Hergt, A., Grund, S., Flamm, J., Lejon, M., and Sahota, H. "On the Secondary Flow System of an Aggressive Inter Compressor Duct." *Journal of Turbomachinery* Vol. 146 No. 10 (2024). DOI 10.1115/1.4065242.

[2]   Naylor, Edward M. J., Ortiz Dueñas, Cecilia, Miller, Robert J., and Hodson, Howard P. "Optimisation of Non-Axisymmetric Endwalls in Compressor S-Shaped Ducts.". *Volume 6: Turbomachinery, Parts A, B, and C*: pp. 305–316. Berlin, Germany, 09.06.2008 - 13.06.2008. DOI 10.1115/GT2008-50448.

[3]   Karakasis, Marios K., Naylor, Edward M. J., Miller, Robert J., and Hodson, Howard P. "The Effect of an Upstream Compressor on a Non-Axisymmetric S-Duct.". *Volume 7: Turbomachinery, Parts A, B, and C*: pp. 477–486. Glasgow, UK, 14.06.2010 - 18.06.2010. DOI 10.1115/GT2010-23404.

[4]   Stürzebecher, Thomas, Goinis, Georgios, Voss, Christian, Sahota, Harsimar, Groth, Pieter, and Hammer, Steffen. "Automated aerodynamic optimization of an aggressive S-shaped intermediate compressor duct.". *Turbo Expo: Power for Land, Sea, and Air*: V02DT46A002.

[5]   Kasper, Aaron, Hergt, Alexander, Stürzebecher, Thomas, Grund, Sebastian, Flamm, Jasmin, and Nicke, Eberhard. "Flow Structure within an Aggressive S-Shaped Intermediate Compressor Duct." *Journal of Physics: Conference Series* Vol. 1909 No. 1 (2021): p. 12025. DOI 10.1088/1742-6596/1909/1/012025.

[6]   Dygutsch, T., Kasper, A., and Voss, C. "On the effect of inter compressor duct length on compressor performance." *The Aeronautical Journal* Vol. 126 No. 1302 (2022): pp. 1333–1350. DOI 10.1017/aer.2022.51.

[7]   Walsh, Philip P. and Fletcher, Paul. *Gas turbine performance*. Blackwell Science, Oxford (2006).

[8]   Kasper, Aaron, Dygutsch, Thomas, Grund, Sebastian, Beversdorff, Manfred, Hakansson, Sebastian, Nicke, Eberhard, and Lejon, Marcus. "Experimental Investigation of an Aggressive S-Shaped Intermediate Compressor Duct." *Proceedings of ASME Turbo Expo 2022* Vol. 2022 (2022).

[9]   Isak Jonsson, Alexandre Capitao Patrao, Petter Milten, Carlos Xisto, Marcus Lejon. "Experimental and Numerical Study on the Effect of OGV Clocking on ICD Performance." *Proceedings of ASME Turbo Expo 2024* Vol. 2024 (2024).

[10]   Becker, Kai, Heitkamp, Kathrin, and Kügeler, Edmund. "Recent progress in a hybrid-grid CFD solver for turbomachinery flows.". *Proceedings fifth European conference on computational fluid dynamics ECCOMAS CFD*.

[11]   Menter, F. R. "Two-equation eddy-viscosity turbulence models for engineering applications." *AIAA Journal* Vol. 32 No. 8 (1994): pp. 1598–1605. DOI 10.2514/3.12149.

[12]   Langtry, Robin B. and Menter, Florian R. "Correlation-Based Transition Modeling for Unstructured Parallelized Computational Fluid Dynamics Codes." *AIAA Journal* Vol. 47 No. 12 (2009): pp. 2894–2906. DOI 10.2514/1.42362.

[13]   Wallin, Fredrik, Langhoff, Philipp, and Nicke, Eberhard. "Aerodynamic Test Campaign of next Generation Aggressive Intermediate Compressor Ducts." *ISABE 2019* (2019).